TU Delft

Delft University of Technology

Document Version
Final published version

Citation (APA)
Liu, S., Shetgaonkar, A., & Popov, M. (2020). Coordinative performance of HVDC circuit breakers in MTDC grids. In *2020 IEEE Power & Energy Society General Meeting (PESGM)* (pp. 1-5). Article 9281921 IEEE. https://doi.org/10.1109/PESGM41954.2020.9281921

Important note
To cite this publication, please use the final published version (if applicable).
Please check the document version above.

Copyright
In case the licence states “Dutch Copyright Act (Article 25fa)”, this publication was made available Green Open Access via the TU Delft Institutional Repository pursuant to Dutch Copyright Act (Article 25fa, the Taverne amendment). This provision does not affect copyright ownership.
Unless copyright is transferred by contract or statute, it remains with the copyright holder.

Sharing and reuse
Other than for strictly personal use, it is not permitted to download, forward or distribute the text or part of it, without the consent of the author(s) and/or copyright holder(s), unless the work is under an open content license such as Creative Commons.

Takedown policy
Please contact us and provide details if you believe this document breaches copyrights.
We will remove access to the work immediately and investigate your claim.

This work is downloaded from Delft University of Technology.

Green Open Access added to TU Delft Institutional Repository

'You share, we take care!' - Taverne project

https://www.openaccess.nl/en/you-share-we-take-care

Otherwise as indicated in the copyright section: the publisher is the copyright holder of this work and the author uses the Dutch legislation to make this work public.

Coordinative performance of HVDC circuit breakers in MTDC grids

Siyuan Liu, Ajay Shetgaonkar and Marjan Popov, *Senior IEEE Member*

***Abstract*—The objective of this paper is to investigate the coordinative performance of different types of high voltage DC (HVDC) circuit breakers (CBs) in multi-terminal DC (MTDC) grids. Several different HVDC CB technologies are emerging as a solution for the protection of offshore MTDC grids. There is a need for coordinative operation between different types of DC CBs in the same network. In this paper, two typical types of DC CBs are modelled in detail and implemented in a 4-terminal MTDC grid in PSCAD environment, by considering operation time, interruption capability and interruption characteristics. Since the requirement of the DC CBs depends on the magnitude of the interrupted current where they are implemented, the fault scenarios in all terminals are studied and the worst scenarios are selected to demonstrate the coordinative performance of different DC CBs. Four cases are defined and demonstrated by two different types of CBs at each terminal of the cable. DC CBs perform differently with the change of the operating time and the locations where they are implemented. The performances and energy absorption are compared and analyzed. The obtained results can be used as DC CB's selection optimization methodology for future MTDC grids.**

***Index Terms*—HVDC circuit breaker, DC grid protection, offshore windfarm, circuit breaker performance**

I. Introduction

The demands to utilize renewable energy significantly promote the integration of energy transmission systems [1]. MTDC grids provide a feasible solution to utilize the offshore wind farm resources because of the benefits like more operating flexibility and increase in reliability [2]. However, the development of meshed offshore MTDC grids is hindered by a few technical barriers. One of the main barriers is the lack of reliable, fast, low loss and cost-effective HVDC CBs, which can isolate the fault segments of the HVDC grid and keep the other components operating continuously [3].

Extensive studies have been done on the development of HVDC CBs, and several DC CB topologies have been proposed and realized to deal with the protection matters in MTDC grids [4]–[7]. Based on different operating principles, these HVDC CBs can be divide in two categories: hybrid circuit breakers and mechanical circuit breakers. In the hybrid circuit breaker, the main branch comprises a string of series-connected semiconductor devices having turn-off capability (e.g. IGBTs), which eliminates the line current within 3-5 ms [8]. Meanwhile, the series-connected semiconductor devices need to withstand the transient interruption voltage (TIV), which results in relatively high costs. Mechanical circuit breakers, on the other hand, utilize mechanical interrupters to clear the fault current at current zero-crossing. However, the long operation delay of traditional spring-based driving mechanisms cannot meet the fast protection requirements of MTDC grids. The development of ultra-fast actuators based on Tomson's coils makes it possible for mechanical CBs to interrupt the current within 5-8 ms [9]. The different characteristics of hybrid CBs and mechanical CBs are challenging to study the coordinative performance when they are implemented in the same MTDC grid and operate at the same time.

Currently, three MTDC grids are commissioned in China, namely, 160 kV 4 terminal MTDC grid at Nan'ao with active injection mechanical DC CBs [10], 200 kV 5 terminal MTDC grid at Zhoushan with hybrid DC CBs [11] and 500 kV 4 terminal MTDC grid at Zhangbei with different types of DC CBs [12]. The technical performance of one type of HVDC CBs in MTDC grids have been well studied. However, currently no coordinative performance of two different types of HVDC CBs implemented in the same MTDC have been reported in the literature.

This paper investigates the coordinative performance by implementing two types of DC CBs in a four-terminal MTDC grid. The two DC interruption technologies are active injection mechanical DC CB [13], and VSC assisted resonant current (VARC) DC CB [14], respectively. It needs to point out that these two types of DC CBs implemented in the MTDC are only used to represent the mechanical DC CB and hybrid DC CB, and the comparison of interruption characteristics of these two CB topologies is not the objective of this paper. The maximum fault current in each terminal of the MTDC depends on the fault type, fault impedance, fault duration and the amount of supplied power. Therefore, the requirement of DC CB interruption capability at each terminal is also different. Some terminals can endure the fault for a longer period without blocking the Multilevel Modular Converters (MMC), whilst at some other terminals the fault should be promptly cleared in order to keep the MMC working continuously. This paper proposes a solution to optimize the selection of DC CBs in MTDC so that the coordinative operations of different types of DC CB works without blocking MMC.

II. Test 4-terminal MTDC grid description

Fig. 1 shows the four-terminal DC network consisting of two onshore converter stations (MMC 1 and MMC 2) and two offshore converter stations (MMC 3 and MMC 4). In this network, MMC 1, 2 and 4 form a smallest mesh and MMC 3 forms a radial connection.

Onshore AC grid operates at the voltage level of 400kV, and the offshore wind operates at 155 kV. The DC link operating voltage is +/- 320kV. The system configuration is symmetrical monopole with the cable connections. VSC technology is adopted for the converter with a half-bridge VSC type. Distance between MMC 1 and 2 is 175 km. Moreover, the distance between MMC 1 and 4 is about 300

This work has received funding from the European Commission under project 691714 – PROMOTioN (Progress on Meshed HVDC Offshore Transmission Networks) through Horizon 2020 program."

S. Liu is with the State Key Laboratory of Electrical Insulation and Power Equipment, Department of Electrical Engineering, Xi'an Jiaotong University, 710049, Xi'an, China, and with the Delft University of Technology, Faculty of EEMCS, Mekelweg 4, 2628CD, Delft, The Netherlands. (e-mail: S.liu-2@tudelft.nl).

A. Shetgaonkar and M Popov are with Delft University of Technology, Faculty of EEMCS, Mekelweg 4, 2628CD, Delft, The Netherlands (e-mail: A.D.Shetgaonkar@student.tudelft.nl; M.Popov@ieee.org).

XXX-X-XXXX-XXXX-X/XX/$XX.00 ©20XX IEEE

978-1-7281-5508-1/20/$31.00 ©2020 IEEE

Authorized licensed use limited to: TU Delft Library. Downloaded on December 17,2020 at 13:44:35 UTC from IEEE Xplore. Restrictions apply.

km. Two onshore converters i.e. MMC 1 and 3 are separated with a distance of 350 km. The distance between MMC 2 and 4 is smallest i.e. 100 km. DC CBs are placed at each end of the line. The nomenclature of the line is given based on the starting and termination end, for example, Cable 12 indicates a cable that begins from the bus at MMC 1 and ends up at the bus at MMC 2.

The data of the four-terminal MTDC system is shown in Table 1, and it is modelled in PSCAD environment. The fault types, the fault location, the fault impedance, and the fault duration are all adjustable. The MMC converters will be blocked when the voltage is less than 0.8 p.u and arm current exceeds 1.6 p.u.

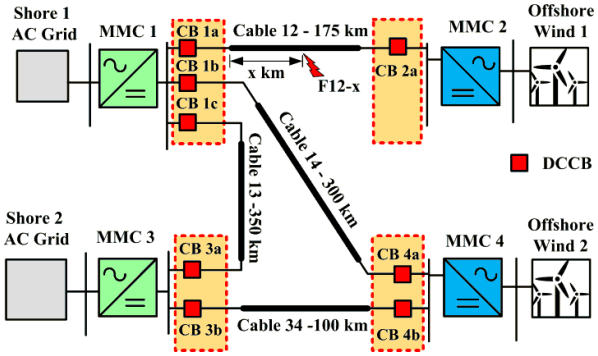

Fig. 1 Test 4 - terminal MTDC system

Table 1 Data of MMCs in 4 - terminal MTDC system

Parameter	Converters			
	MMCs 1	MMC 2	MMC 3	MMC 4
Active power	500 MW	500 MW	500 MW	500 MW
Control mode	PVdc	PQ	PVdc	PQ
Reactive power	100 MVAR	100 MVAR	100 MVAR	100 MVAR
DC link Voltage	±320 kV			
Rated power	1256 MW			
Number of Submodules per arm	400			
Arm capacitance C_{arm}	22 µF			
Arm indcutance L_{arm}	42 mH			
Arm resistance R_{arm}	0.544 Ω			
AC converter voltage	400kV			
Transformer leakage reactance	0.18 p.u			
AC grids and windfarms				
AC grids voltage	400 kV			

III. Considered Types of DC CB

A. *Topologies of typical DC CBs*

Fig. 2 illustrates the structure of the mechanical DC CB with current injection. The model of this DC CB is described in detail in [1], and the DC CB prototype has been tested in [15].

Fig. 3 shows the structure of the VARC DC, which is proposed in [15]. The detailed model has been verified by the experimental results performed at KEMA laboratories [15].

B. *Operating principle and timing sequence*

Fig. 4 shows the current and the voltage waveforms of the VARC DC CB and the mechanical DC CB during the interruption where I_{line} is the current through the DC CB, I_{vi} is the current through the vacuum interrupter (VI), I_{sa} is the current through the energy absorption branch, and V_{vi} is the voltage across the VI. L_{DC} is chosen to limit the rising rate of the fault current with the value of 100 mH based on [14], the same L_{DC} value is applied in both types of DC CBs. The detailed operation sequence for both circuit breaker topologies is explained as follows:

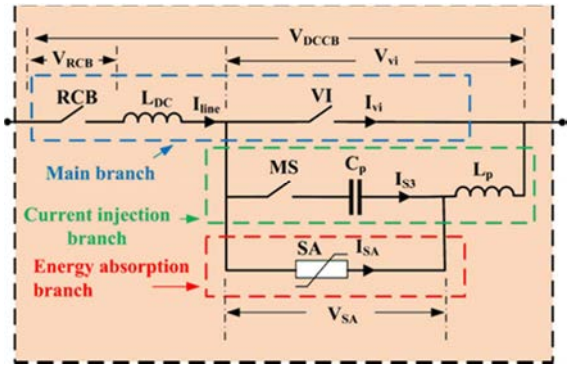

Fig. 2 Configuration of Mechanical Circuit breaker

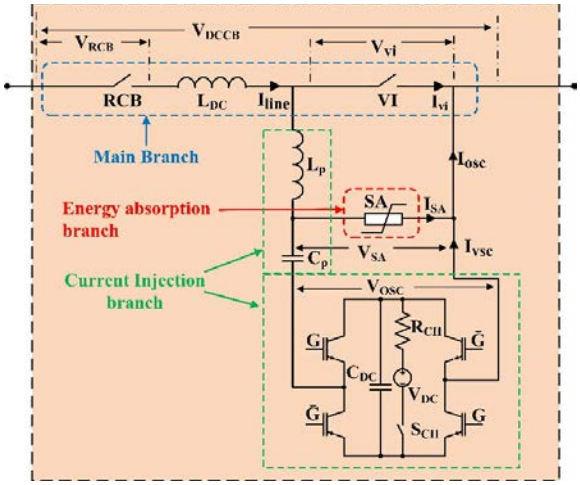

Fig. 3 Configuration of VARC Circuit breaker

t_0 - t_1: Before the operation of the DC CB, the VSC energy storage capacitor (C_{DC}) is pre-charged by the charging circuit in VARC. For the mechanical DC CB, capacitor (C_P) in the oscillating circuit is charged to the system voltage level by the charging circuit.

t_1 – t_2: A fault occurs at instant t_1. As a result, the line current begins to rise, and the rate-of-rise of the line current is limited by the fault current limiting reactor (L_{DC}). At instant t_2, a trip signal is sent to both DC CBs at the ends of the faulty cable.

t_2 – t_{2a}: The VARC DC CB receives the trip signal at t_2, and the ultra-fast actuator starts to drive the separation of contacts. The contacts in the VI reach a sufficient gap distance to withstand the TIV at t_3.

t_{2a} – t_3: Shortly before the VI reaches sufficient contact separation at t_{2a}, the VSC is activated. The oscillating current is generated, and its amplitude gradually increases every half cycle until a zero-crossing is created in the arc current in VARC DC CB. The special characteristic of VI make it possible to clear the fault current at zero-crossing.

t_3 – t_4: The VI stops conducting at t_3 in both DC CBs. As the VI is connected in parallel to the oscillation branch, the initial transient interruption voltage (ITIV) across VI equals the remaining voltage of the current injection branch capacitor. At the same time, the line current is commutated to the current injection branch. During t_3 – t_4, the system

Authorized licensed use limited to: TU Delft Library. Downloaded on December 17,2020 at 13:44:35 UTC from IEEE Xplore. Restrictions apply.

keeps charging the current injection branch capacitor, until its voltage reaches the clamping voltage of SA at t_4.

$t_4 – t_5$: The SA begins to conduct at t_5, and the line current is commutated into the energy absorption branch. The SA current then decreases until it drops to zero at t_6.

$t_5 – t_6$: After the fault current interruption, some leakage current may exist in the system, as well as a low-frequency interaction between the capacitor in the circuit breaker and the inductance connected in series with the breaker. The residual circuit breaker is opened at t_7 to clear the leakage current and separate the breaker main circuit from the grid.

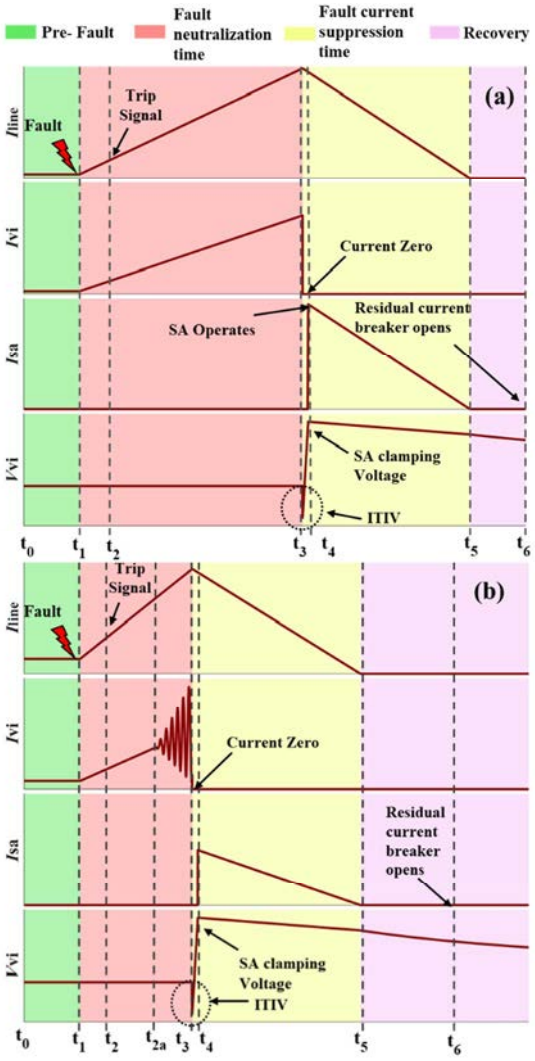

Fig. 4 Voltage and current waveforms of the (a) Mechanical DC CB (b) VARC DC CB.

IV. Fault Case

In order to analysis the coordinative performance of the DC CB, the DC fault is analysed. The analysis of the DC fault cases is based on the type of fault, location of the fault and fault neutralization time. Fault neutralization time referred to as the operation delay in further text. The fault location is considered in terms of percentage of the cable length. Fig. 5 illustrates the fault case scenarios performed in the test topology. The type of the fault is denoted as PP and PG representing pole to pole fault and pole to ground fault respectively. Due to similar results produced, pole to pole to ground fault is not considered. The terminology used in the plot is, for example, PP12 3ms indicating pole to pole fault on cable12 where 1 is the starting and 2 is the ending node of cable with 3 ms operation delay.

When analysing the fault case scenarios, it can be seen that the faulty cable 12 has a larger fault current amplitude especially a fault location near bus 1; this is due to the power which is fed from MMC 3 and MMC 4 at bus 1. Similarly, the fault current amplitude is considerably high in cable 13 and 14. As it is shown in Table 2, the worst-case scenarios are always cable 12 and 13. Hence, a fault in cable 12 and 13 is analysed for the selection of breaker.

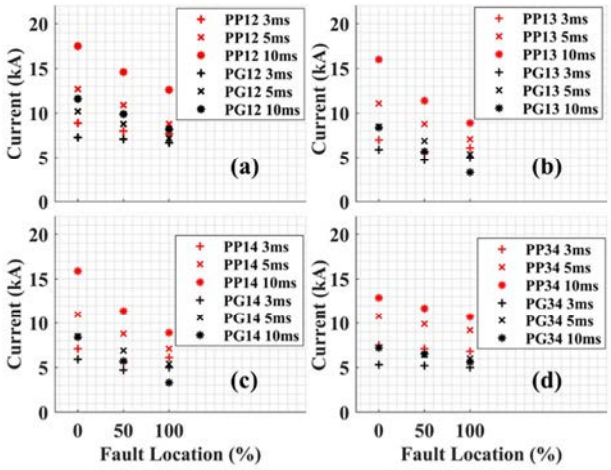

Fig. 5 Results of the possible pole to pole and pole to ground faults with different operation time in test topology; (a) fault in cable 12 (b) fault in cable 13 (c) fault in cable 14 and (d) fault in cable 34

Table 2 Maximum fault current in a cable (worst scenarios in red)

Location	Case 1	Case 2	Case 3	Case 4
Cable 12	13.11 kA	16.72 kA	13.11 kA	8.69 kA
Cable 13	11.38 kA	15.07 kA	11.38 kA	7.3 kA
Cable 14	11.18 kA	14.8 kA	11.18 kA	7 kA
Cable 34	10.7 kA	12.1 kA	10.7 kA	7.5 kA

V. Results and Analysis

Based on the fault case scenarios in Section IV, 4 cases are carried out on the worst fault cable 12 and cable 13, with two typical DC CBs at each end of the faulty cable. The following case studies are conducted on the Multi-terminal terminal network. In the cases below, i and j represent the start and endpoint of cable.

- ***Case 1***: Mechanical DC CB with 5 ms operational delay is introduced at the bus of MMC i and VARC DC CB within 3 ms operational delay is introduced at the bus of MMC j.
- ***Case 2***: Mechanical DC CB with 8 ms operational delay is introduced at the bus of MMC i and VARC DC CB with 3 ms operation delay is introduced at the bus of MMC j.
- ***Case 3***: Mechanical DC CB with 5 ms operational delay is introduced at the bus of MMC i and Mechanical DC CB with 5 ms operational delay is introduced at the bus of MMC j.
- ***Case 4***: VARC DC CB with 3 ms operational delay is introduced at the bus of MMC i and VARC DC CB with 3 ms operation delay is introduced at the bus of MMC j.

Authorized licensed use limited to: TU Delft Library. Downloaded on December 17,2020 at 13:44:35 UTC from IEEE Xplore. Restrictions apply.

A. *Interruption performance*

Fig. 6 shows the current and the voltage waveforms in CB 1a for the pole to pole fault on cable 12 near MMC 1. The I_{line} in case 2 has the most considerable magnitude of the current due to slower breaking near MMC 1. The effect of the travelling wave is not as significant as the fault located near CB 1a. Hence, the rise of the fault current is linear. During the interruption, in case 2, as the capacitor charged with opposite polarity causes a rise of the current up to 34 kA in VI. However, in the case of VARC CB this rise reaches up to 18kA with a high frequency growing oscillation in VI. During the fault current suppression, the time is determined based on the interrupted current. Hence, VARC has the least fault current suppression time as compared to a mechanical circuit breaker with an operational delay of 8ms. The voltage across the VI after, during the fault current suppression time remains the same for all the cases. Moreover, the amplitude of ITIV depends on the magnitude of the current in VI. For the mechanical CB, the higher current is interrupted, the lower is the ITIV [1]. There is a significant oscillation in the V_{vi} for all cases except for case 2 after the fault current zero.

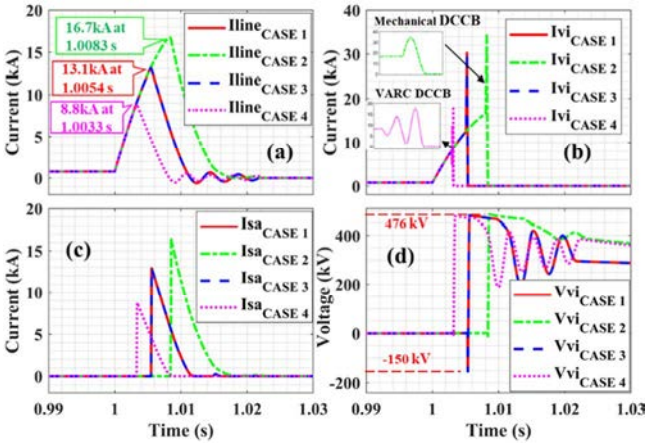

Fig. 6 Current and voltage waveforms in CB 1a in various cases. (a) Current (in kA) though DC CB. (b) Current (in kA) though the vacuum interrupter (VI). (c) Current (in kA) though the surge arrester (SA). (d) Voltage (in kV) across the VI.

The fault located near MMC 1 has an effect on the current and the voltage waveforms in CB 2a as depicted in Fig. 7, For I_{line}, the effect of travelling waves is visible and it changes the fault current rise rate non-linearity. For case 3, as the presence of the mechanical circuit breaker with an operational delay of 5ms has peak amplitude of 6.9 kA at 1.0064 s. It is observed that during the fault current suppression time for case 1,2 and 4, the drop of current is non-linear, and this is due to the travelling wave phenomena. However, the effect is not seen in case 3. Significantly large ITIV is observed for case 3 with an amplitude of -260 kV.

For a fault that occurs in cable 13 near the MMC 1, identical waveforms are observed primarily in CB 1b. However, due to the same charging of the DC capacitor for the mechanical DC breaker, there is no overshoot as it can be seen in CB 1a for current I_{vi}.

Furthermore, significant changes can be seen in CB 3a as depicted in Fig. 8. For case 2, the fault current rises to 8.4 kA due to the presence of a mechanical circuit breaker with an operational delay of 5 ms. Similarly, the fault current is quickly damped after the current zero. A non-linearity is observed in the SA current due to travelling waves as the distance is considerable, i.e. 350 km, however, case 3 is severely affected by it. The oscillation in V_{vi} after the current zero reaches lower amplitude as compared to Fig.6.

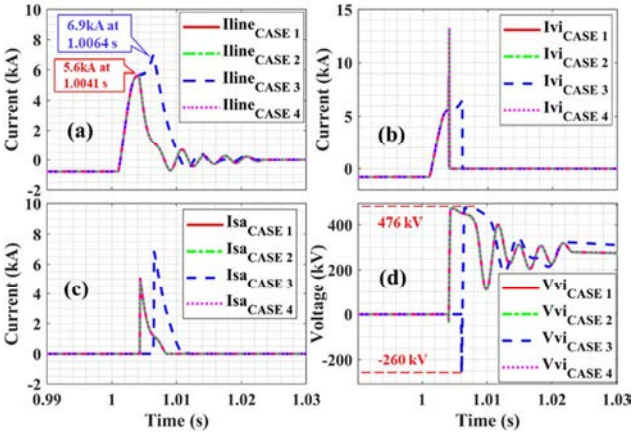

Fig. 7 Current and voltage waveforms in CB 2a in various cases. (a) Current (in kA) though DC CB. (b) Current (in kA) though the vacuum interrupter (VI). (c) Current (in kA) though the Surge arrester (SA). (d) Voltage (in kV) across the VI

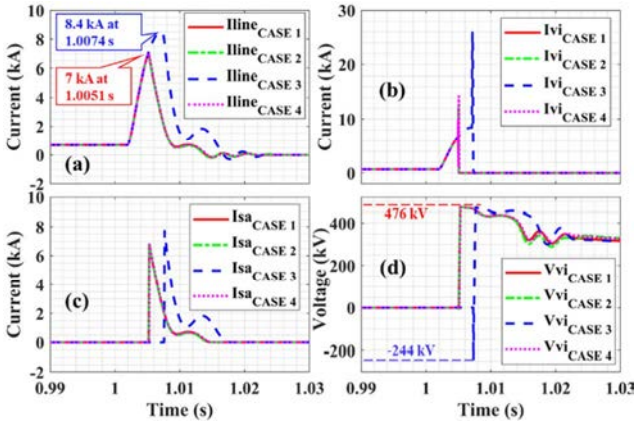

Fig. 8 Current and voltage waveforms in CB 3a in various cases. (a) Current (in kA) though DC CB. (b) Current (in kA) though the vacuum interrupter (VI). (c) Current (in kA) though the SA. (d) Voltage (in kV) across the VI.

B. *MMC's Blocking Status*

Table 3 illustrates the blocking status of the MMC. It is observed that among all the cases, for various fault locations case 1 and case 4 do not block the converter. However, it is interesting to see that a fault that occurs on line 34 is mitigated for all cases except for case 2. This is due to the fact that the power flow between MMC 3 and MMC 4 is zero during the steady state. Hence, there is sufficient time for the current to reach the fault location.

Table 3 Blocking status of MMC for various case scenarios

Location	Case 1	Case 2	Case 3	Case 4
Cable 12 - 0	-	MMC 1	-	-
Cable 12 - 50	-	MMC 1	-	-
Cable 12 - 100	-	-	MMC 2	-
Cable 13 - 0		MMC 1	-	-
Cable 13 - 50	-	-	-	-
Cable 13 - 100	-	-	MMC 3	-
Cable 14 - 0	-	MMC 1	-	-
Cable 14 - 50	-	-	MMC 1	-
Cable 14 – 100	-	-	MMC 4	-
Cable 34 - 0	-	-	MMC 4	-
Cable 34 - 50	-	-	MMC 4	-

Authorized licensed use limited to: TU Delft Library. Downloaded on December 17,2020 at 13:44:35 UTC from IEEE Xplore. Restrictions apply.

Cable 34 - 100	-	-	MMC 4	-

C. Energy absorption

The total energy absorption by the SA consists of two sources, magnetic energy stored in the DC current limiter and the energy stored in the system. The energy stored in the DC current limiter is $\frac{1}{2}L_{DC}I_f^2$; the electrical energy supplied from the system during the fault current suppression. In some cases, the energy resulting from the grid side is even larger than the energy stored in the DC current limiter because of the system voltage recovery during the energy period. Fig. 9 shows the energy absorption by the DC CB's at a different location for various case scenarios during pole to pole fault. The amount of energy absorbed depends on the operational speed of the DC CB, as case 4 shows the fastest topology, it absorbs less energy than other cases. The energy absorption with different fault location is nearly constant. Similarly, in Case 3 the converter is not blocked, and the maximum energy absorbed by the SA is below 16 MJ.

For the selection of the DC CB technology based on the energy absorbed, a line can be drawn. A faster case i.e. case 4 can be used for cable 12 as the energy absorption difference between the opposite breakers (CB 1a and CB 2a) is larger. However, for cable 13 and cable 14, the difference in the absorbed energy is smaller, hence case 1 is found as suitable and similarly, for cable 34, case 2 can be used.

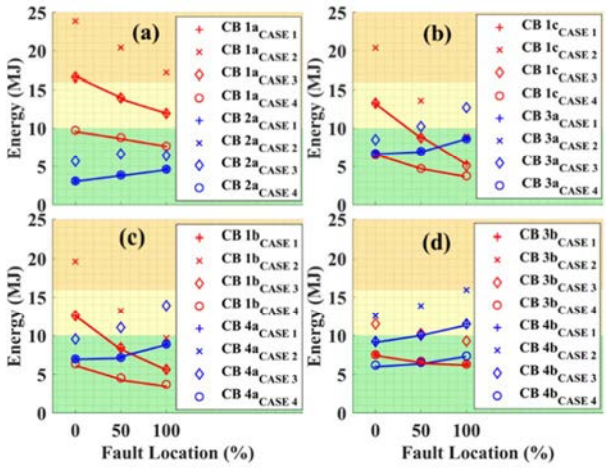

Fig. 9 Energy absorbed in the grid by DC CB's during various case scenarios in (a) Cable 12. (b) Cable 13. (c) Cable 14. (d) Cable 34.

D. Selection of DC CBs

The selection of DC CBs for the specific MTDC should consider the maximum fault current, MMC blocking feature, operational delay of the breaker and the energy absorption. Since the requirement of the DC CBs depends on the magnitude of the interrupted current where they are implemented, for some terminals with a high rate of rise of the fault current, the application of fast VARC DC CBs are essential. On the other hand, for other terminals, when the mechanical DC CBs interrupt the fault without the blocking of the MMC converters, the combination of VARC DC CBs and mechanical DC CBs may reduce the cost of the MTDC protection system.

VI. Conclusion

The paper presents a coordinative performance of an active injection mechanical DC CB and a VARC DC CB for a 320 kV 4-terminal MTDC grid. The worst-case scenario of a fault occurs for cable 12 and 13, when the fault is near the converter station. The coordinative performance of two types of DC CBs are demonstrated accordingly. For case 1, the combination of a mechanical DC CB and a VARC DC CB with an operational delay of 5ms and 3 ms respectively can successfully clear the fault without blocking the MMC converters. For case 4, VARC DC CBs installed at remote terminals can interrupt the fault.

The amount of energy absorption depends on the operational times and the type of DC CB, and the energy absorber should be designed accordingly. The coordinative operation of the DC CBs is very important as a possible failure at any DC CB may lead to the blocking of the converters. The methodology proposed in this paper can be applicable to other MTDC configurations in the future.

VII. Reference

[1] S. Liu, Z. Liu, J. de Jesus Chavez, and M. Popov, "Mechanical DC circuit breaker model for real time simulations," *Int. J. Electr. Power Energy Syst.*, vol. 107, pp. 110–119, May 2019.

[2] S. Rodrigues, R. T. Pinto, P. Bauer, and J. Pierik, "Optimal Power Flow Control of VSC-Based Multiterminal DC Network for Offshore Wind Integration in the North Sea," *IEEE J. Emerg. Sel. Top. Power Electron.*, vol. 1, no. 4, pp. 260–268, 2013.

[3] N. A. Belda, C. A. Plet, and R. P. P. Smeets, "Analysis of Faults in Multiterminal HVDC Grid for Definition of Test Requirements of HVDC Circuit Breakers," *IEEE Trans. Power Deliv.*, vol. 33, no. 1, pp. 403–411, 2018.

[4] L. Ängquist, S. Nee, T. Modeer, A. Baudoin, S. Norrga, and N. A. Belda, "Design and test of VSC assisted resonant current (VARC) DC circuit breaker," in *The 15th IET international conference on AC and DC Power Transmission*, 2019, pp. 1–6.

[5] Bucher, Matthias K, and Christian M. Franck. "Fault current interruption in multiterminal HVDC networks." *IEEE Trans on Power Delivery* vol. 31.1 (2015): 87-95.

[6] S. Tokoyoda *et al.*, "Interruption characteristics of vacuum circuit breaker and the application to DC CB," 13th IET International Conference on AC and DC Power Transmission 2017, pp. 1–5.

[7] W. Zhou *et al.*, "Development and test of a 200kV full-bridge based hybrid HVDC breaker," in *2015 17th European Conference on Power Electronics and Applications,* 2015, pp. 1–7.

[8] J. Meyer and A. Rufer, "A DC hybrid circuit breaker with ultra-fast contact opening and integrated gate-commutated thyristors (IGCTs)," *IEEE Trans. Power Deliv.*, vol. 21, pp. 646–651, 2006.

[9] B. Zhang *et al.*, "A Relationship between Minimum Arcing Interrupting Capability and Opening Velocity of Vacuum Interrupters in Short-circuit Current Interruption," *IEEE Trans. Power Deliv.*, vol. 8977, no. c, pp. 1–7, 2018.

[10] H. Rao, "Architecture of Nan'ao multi-terminal VSC-HVDC system and its multi-functional control," *CSEE J. Power Energy Syst.*, vol. 1, no. 1, pp. 9–18, 2015.

[11] G. Tang, Z. He, H. Pang, X. Huang, and X. Zhang, "Basic topology and key devices of the five-terminal DC grid," *CSEE J. Power Energy Syst.*, vol. 1, no. 2, pp. 22–35, 2015.

[12] X. Han, W. Sima, M. Yang, L. Li, T. Yuan, and Y. Si, "Transient Characteristics Under Ground and Short-Circuit Faults in a 500 kV MMC-Based HVDC System With Hybrid DC Circuit Breakers," *IEEE Trans. Power Deliv.*, vol. 33, no. 3, pp. 1378–1387, 2018.

[13] K. Tahata *et al.*, "HVDC circuit breakers for HVDC grid applications," *11th IET International Conference on AC and DC Power Transmission*, Birmingham, 2015, pp. 1-9.

[14] S. Liu *et al.*, "Modelling, Experimental Validation and Application of VARC HVDC Circuit Breakers," *IEEE Trans. Pow Deliv.* 2019.

[15] N. A. Belda, C. Plet, and R. P. P. Smeets, "Full-Power Test of HVDC Circuit-Breakers with AC Short-Circuit Generators Operated at low Power Frequency," *IEEE Trans. Power Deliv.*, 2019.

Authorized licensed use limited to: TU Delft Library. Downloaded on December 17,2020 at 13:44:35 UTC from IEEE Xplore. Restrictions apply.